Available online at www.sciencedirect.com
ScienceDirect
Cement and Concrete Research 38 (2008) 337–349
Cement and Concrete Research

A thermodynamic and experimental study of the conditions of thaumasite formation

Thomas Schmidt [a,*], Barbara Lothenbach [a], Michael Romer [a,c], Karen Scrivener [b], Daniel Rentsch [a], Renato Figi [a]

[a] Empa, Swiss Federal Institute for Material Testing and Research, 8600 Dübendorf, Switzerland
[b] EPFL, Swiss Federal Institute of Technology, Laboratory of Construction Materials, 1015 Lausanne, Switzerland
[c] Holcim Group Support Ltd, 5113 Holderbank, Switzerland

Received 25 May 2007; accepted 4 November 2007

Abstract

The formation of thaumasite was investigated with the progressive equilibrium approach (PEA). This approach experimentally simulates the conditions of various levels of sulfate addition in hardened cement pastes. The influence of limestone, time, C_3A content, temperature and leaching on thaumasite formation was investigated. The results show that thaumasite formation is favoured at lower temperatures (8 °C) independently of the type of cement clinker (high or low C_3A content) used. Thaumasite was found to form only in systems where limestone was present and where sufficient sulfate had been added. Thaumasite precipitated only in systems where the Al present has already been consumed to form ettringite and the molar SO_3/Al_2O_3 ratio exceeded 3. In leached samples (reduction of portlandite and alkalis) slightly less thaumasite was formed whereas gypsum and ettringite are favoured under these conditions. The PEA, used to investigate the chemical aspects of sulfate attack was found to be a good tool for simulating external sulfate attack. Generally, thaumasite was detected were it was modelled to be stable in significant amounts. However, in this study equilibrium conditions were not reached after 9 months.

Keywords: Thaumasite; Sulfate attack; Leaching; Temperature; Thermodynamic modelling

1. Introduction

Sulfate attack in mortars and concretes causes the formation of sulfate containing phases such as ettringite ($3CaO \cdot Al_2O_3 \cdot 3CaSO_4 \cdot 32H_2O$) and gypsum ($CaSO_4 \cdot 2H_2O$), which may lead to expansion. However, in cements and concretes containing a source of carbonate the formation of thaumasite ($CaSiO_3 \cdot CaCO_3 \cdot CaSO_4 \cdot 15H_2O$) can also be observed.

In recent years thaumasite formation has been studied and some risk factors have been identified [1]. The thaumasite form of sulfate attack requires a source of calcium silicate, sulfate, carbonate and excess of humidity [2–5].

It has been found that thaumasite is more stable at lower temperatures. It has been suggested by Bensted [2,3] that silicon tends to adopt the octahedral co-ordination found in thaumasite more easily at lower temperatures. Nevertheless, thaumasite is formed also at temperatures around 20 °C and above as reported for buildings in Southern California [6] and Italy [7]. Once thaumasite has formed it remains stable up to 30 °C [8].

Thaumasite has been found in cement systems with both high and low C_3A contents [9–11]. Thaumasite itself contains no alumina but it has been proposed that the presence of aluminium promotes thaumasite formation [11]. In contrast, Blanco-Valera et al. [9] found that low C_3A cements produce higher amounts of thaumasite.

The formation of thaumasite needs a source of carbonate which can be supplied from the limestone contained in the cement itself [12], from carbonate containing aggregates, ground waters [13], soils [5] or the air (CO_2) [14]. The presence of limestone used as filler in cement has been found to influence the type of AFm phase present; monocarbonate ($C_3A \cdot CaCO_3 \cdot 11H_2O$) forms instead of monosulfate ($C_3A \cdot CaSO_4 \cdot 12H_2O$) in the presence of calcite [15].

* Corresponding author. Tel.: +41 21 6932852; fax: +41 21 6935800.
E-mail address: thomas.schmidt@epfl.ch (T. Schmidt).

0008-8846/$ - see front matter © 2007 Elsevier Ltd. All rights reserved.
doi:10.1016/j.cemconres.2007.11.003

Table 1
Composition of the laboratory cements before a) and after b) the leaching process and of the limestone filler used in the study

Chemical composition [wt.%]							
	a) Initial			b) Leached[a]			
	HS	OPC	Limestone	HS		OPC	
SiO_2	19.2	20.1	0.05	19.2	(±0)	20.1	(±0)
Al_2O_3	4.7	4.4	0.10	4.7	(±0)	4.4	(±0)
Fe_2O_3	7.2	2.7	0.02	7.0	(−3)	2.6	(−3)
CaO	62.2	63.7	55.9	34.6	(−44)	38.2	(−40)
MgO	1.5	1.6	0.16	1.5	(±0)	1.5	(−6)
K_2O	1.1	0.9	0.01	0.01	(−99)	0.02	(−98)
Na_2O	0.13	0.15	0.01	0.01	(−92)	0.01	(−93)
SO_3	1.9	2.9	0.01	1.7	(−11)	2.7	(−7)
CO_2	0.1	0.2	43.7	0.4	(+300)	0.5	(+150)
CaO_{free}	0.6	0.9					
LOI	0.7	1.2					
Total	99.3	98.8	99.9				
Surface area [cm^2/g]	3500		5800				
Mineralogical composition [wt.%][b]							
C_3S	62	66					
C_2S	9	10					
C_3A	0.4	7					
C_4AF	22	8					

[a] Normalized to the SiO_2− content (difference in % to initial content).
[b] According to Bogue calculation.

Thaumasite has been observed in the presence and absence of portlandite. It was found that alkaline conditions (pH ≥ 12.5) enhanced thaumasite formation [16], while during strong leaching at low pH levels (pH ≤ 8.0) gypsum became the dominant sulfate phase and the amount of thaumasite decreased [17]. However, Gaze and Crammond [18] showed that once thaumasite forms, it remained stable at pH levels as low as 6–8.

Besides a source of carbonate, high amounts of sulfate are a prerequisite for the formation of thaumasite. It was found that both the addition of gypsum [19] or the presence of a sulfate rich solution [20,21] can lead to thaumasite formation in carbonate containing cements.

However, the mechanisms of thaumasite formation are not known in detail. In the present paper the influence of temperature, internal carbonate, sulfate concentration and pH on the formation of thaumasite are investigated. The present investigation uses the progressive equilibrium approach PEA to evaluate experimentally the mechanisms of thaumasite formation and compares the experimental results with thermodynamic calculations.

2. Materials and methods

2.1. Laboratory cements and cement pastes

The experiments were performed using laboratory cements which were prepared from industrial cement clinkers representing sulfate resistant Portland cement, HS (low C_3A), and ordinary Portland cement, OPC (high C_3A). Pure analytical gypsum was used to adjust the appropriate sulfate contents for HS (SO_3 = 1.9 wt.%) and OPC (SO_3 = 2.9 wt.%) laboratory cement (Table 1). To study the effect of limestone on thaumasite formation the cements remained unchanged, without limestone addition (H0, P0), or were blended by replacing 5 wt.% (H5, P5) and 25 wt.% (P25) of the cement (clinker and gypsum) with natural limestone. The cements H0 and H5 were prepared from HS, the cements P0, P5 and P25 from OPC.

The cement pastes were produced at a water/binder ratio of 0.35 and fabricated as prisms of 40 × 40 × 160 mm^3 and stored for 24 h at 20 °C and 90% relative humidity. After demoulding, the prisms were cured for 56 days in saturated limewater at 20 °C. The hydrated cement paste was then crushed to enhance the specific surface available for the sulfate interaction. The fraction 0.5–2 mm was used for the experiments.

Artificially leached cement paste was prepared from the crushed cement paste samples. 70 g of crushed cement paste were equilibrated in polyethylene containers with 20 l of deionised water and left at 20 °C for 4 months. After 14, 28, 56 and 112 days the leaching water was exchanged with fresh deionised water. A slight uptake of CO_2 during leaching was observed from the CO_2 present in the deionised water and from CO_2 ingression in the polyethylene containers during leaching.

2.2. Progressive equilibrium approach PEA

The progressive equilibrium approach (PEA) was used to investigate the chemical aspects of sulfate attack. The idea of the PEA is to simulate the chemical gradient which can be found in reality on concrete structures undergoing an external sulfate attack over an extended period of time. The chemical gradient is due to a diffusive mass exchange involving external sulfate. The PEA method eases the systematic investigation of the influence of e.g. sulfate addition on the hydrate assemblages. The PEA defines and subsequently simulates fixed chemical subsystems. These subsystems (A–E, sulfate interaction) and (BL–DL, leached sulfate interaction) were set up as closed batch experiments with the aim to minimize the influence of diffusion with fixed sulfate concentrations as shown in Fig. 1.

The amount of sulfate addition varies from 20, 10, 5, 2.5 wt.% SO_4^{2-} by mass cement paste in subsystems A to D down to 0 wt.% SO_4^{2-} in subsystem E, corresponding to sulfate concentrations of 0.30, 0.15, 0.07, 0.04 and 0 mol/l. For the sulfate interaction after the leaching process the addition of the sulfate varies from 10, 5 to 2.5 wt.% SO_4^{2-} in the corresponding subsystem BL, CL and DL, respectively.

For each subsystem duplicate samples of the crushed cement paste (10 g dried at 40 °C for 2 days) were immersed in 70 ml of aqueous reaction solution which was prepared by dissolving adequate amounts of Na_2SO_4 in deionised water. The experiments were then processed as closed subsystems with a liquid/solid ratio of 7 in sealed plastic containers at 8 and 20 °C for 3 and 9 months. The plastic containers were shaken frequently.

2.3. Analytic methods

The chemical composition of the cements was analysed by X-ray fluorescence (XRF, Philips PW 2400). The porosity of

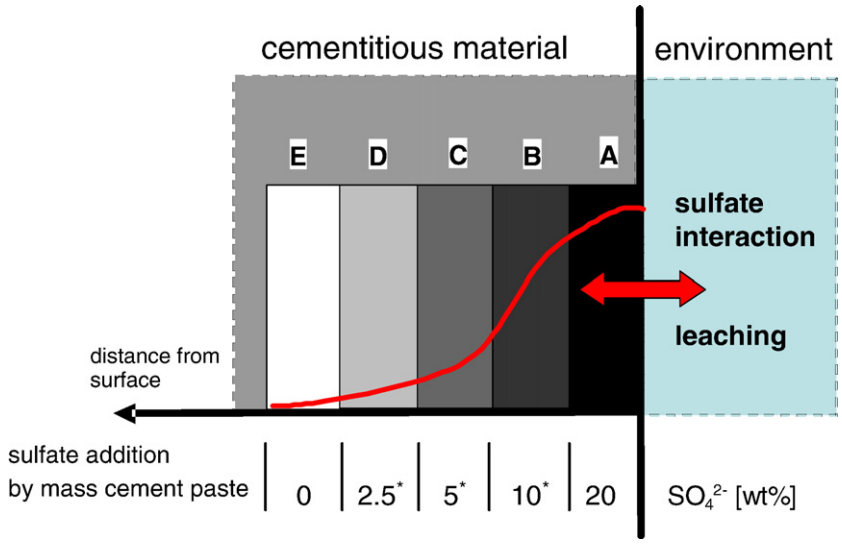

Fig. 1. Schematic illustration of the concept for the progressive equilibrium approach (PEA) * sulfate concentration also used in leached subsystems.

the initial and the leached cement pastes was determined by using Mercury intrusion porosimetry (MIP, Thermoelectron Pascal 140/440). Thermogravimetric analysis (TGA, Mettler Toledo TGA/SDTA851e) was carried out under N_2 on about 10 mg of dried (40 °C), ground cement pastes (≤40 μm) at 20 °C/min from 30 to 980 °C. The amount of portlandite present in the cement pastes initially and after leaching was calculated from the weight loss between 420–500 °C. After 3 and 9 months equilibration time, the liquid and solid phase were separated using 45 μm nylon membrane filters. A part of the undiluted solution was used to determine the pH immediately with a pH electrode (Knick pH-Meter 766 with a Knick SE pH 7Pt 1000 electrode). The electrode was calibrated with 0.1 to 1.0 M KOH solutions. For further analysis 1 ml of pore solution was diluted with 9 ml of 6.5% HNO_3 solution and stored at 5 °C till further analysis. The concentration of Al, S (total sulfur), Ca, K and Na were determined using inductively coupled plasma optical emission spectrometry (ICP-OES, Varian, VISTA Pro); carbonate was determined as total inorganic carbon (TIC, Shimadzu TOC-5000A). The solid residue was immersed for 15 minutes in acetone and the samples then dried for 2 days at 40 °C. For X-ray diffraction (XRD) studies the samples were ground to ≤40 μm and stored in a desiccator at 20 °C. For XRD the samples were analysed by with a PANalytical X'pert PRO diffractometer using CuKα radiation. Unground pieces of the exposed pastes were also examined by scanning electron microscopy (Philips ESEM FEG XL 30) using backscattered electron images and energy dispersive X-ray (EDX) analysis. These samples were prepared by pressure impregnation with epoxy resin, cutting, polishing and coating with carbon.

The NMR experiments were performed on a Bruker Avance 400 NMR spectrometer using a 7 mm CP/MAS probe. The ^{29}Si CP/MAS NMR spectra were recorded at 79.49 MHz using the following parameters: 3000 Hz spinning speed, 800 μs contact time, 6 s relaxation delay for cement mixtures and 60 s for mineral thaumasite (^{29}Si chemical shifts referenced to an external of tetramethylsilane). The quantities of thaumasite were determined using the method described in detail by Skibsted et al. [22,23] with field strengths of 31.2 kHz during the polarisation transfer and 41.6 kHz for the 90° ^1H excitation pulse and during the decoupling sequence. A sample of natural thaumasite originating from Akschal (Kazakhstan) was found to be almost 100% pure (XRD and TGA). The relaxation times T_1^H and $T_{1\rho}^H$ were determined using standard Bruker pulse programs and processing software. For the mineral thaumasite $T_1^H \approx 8$ s was determined, this value decreased to 1 s for cement sample containing Fe^{3+}. The CP build up rates T_{SiH} were determined from least square two-parameter-fits of the CP build up curves for a) Akschal thaumasite, b) 10 wt.% of Akschal thaumasite mixed with 90 wt.% of hydrated cement powder and c) thaumasite formed in a mortar sample after 1.5 years at 8 °C. The following pairs of parameters were determined T_{SiH} [ms]/$T_{1\rho}^H$ [ms]: 0.42/3.83 (Akschal thaumasite); 0.55/3.39 (10% Akschal thaumasite) and 0.33/2.60 (thaumasite in mortar). The latter parameters were applied for the quantification of thaumasite determined for all cement samples under investigation. The accuracy of such results is believed to be within +/−15%.

For the 10% Akschal sample 9.7% thaumasite was determined and 6.5% was found in the mortar sample. The ^{29}Si NMR signal could not be measured in the samples made with the HS cements owing to the high iron content. However, XRD indicated that thaumasite was formed in these samples.

3. Thermodynamic modelling

3.1. Modelling approach

Thermodynamic modelling is used to calculate the composition of the stable hydrate assemblage and of the surrounding solution assuming thermodynamic equilibrium. It should be noted that such thermodynamic calculations describe a quasi equilibrium state which the system seeks to reach, while in real systems, as investigated in this paper, equilibrium is often not achieved.

As input to the thermodynamic calculations the composition of the laboratory cements (assuming complete hydration) as given in Table 1 plus the amount of Na_2SO_4 and H_2O added to

the system was used. The hydrate phases which were found to be stable in the investigated systems comprise C–S–H, portlandite, ettringite, thaumasite, monosulfate, monocarbonate, hemicarbonate ($C_3A{\cdot}0.5CaCO_3{\cdot}12H_2O$), calcite, gypsum and hydrotalcite (M_4AH_{10}). For iron the precipitation of iron hydroxide ($Fe(OH)_3$ or FH_3) was assumed. As detailed elsewhere [24,25] C–S–H was calculated as a ideal solid solution between the end-members jennite $C_{1.67}SH_{2.1}$ and tobermorite $C_{0.83}SH_{1.3}$. For the modelling it was considered that the alkalis which originate from the cements and from the Na_2SO_4 solution used, partition between the aqueous solution and the precipitating C–S–H. The uptake of Na and K by C–S–H was calculated using a distribution ratio R_d of 0.42 ml/g [24,25], where $R_d = \frac{c_s w}{c_d s}\left[\frac{ml}{g}\right]$, c_s alkali concentration in the solid phase [mol/l], c_d alkali concentration in the solution [mol/l] and w/s is the water/C–S–H ratio in ml/g.

3.2. Thermodynamic model and data

GEMS [26] is a broad-purpose geochemical modelling code which uses Gibbs energy minimization and computes equilibrium phase assemblage and speciation in a complex chemical system from its total bulk elemental composition. Chemical interactions involving solids, solid solutions, and aqueous electrolyte are considered simultaneously.

Thermodynamic data for aqueous species as well as for many solids were taken from the PSI thermodynamic dataset [27], which has been adapted for the use in GEMS [28]. Solubility products for cement minerals at 25 °C were taken from the compilation of Lothenbach et al., [24] who prepared a consistent thermodynamic dataset for cement minerals (data relevant for the investigated system are reproduced in Table 2).

The Gibbs free energy of formation $\Delta_f G°$ at 25 °C as given in Table 2 is related to the Gibbs free energy of reaction $\Delta_r G° = \sum_i \nu_i \Delta_f G°$ and to the solubility product $K_{S0} = e^{\frac{-\Delta_r G°}{RT}}$; where ν_i are the stoichiometric reaction coefficients, $R = 8.31451$ J/mol/K and T the temperature in K. The apparent Gibbs free energy of formation $\Delta_a G°$ at 8 and 20 °C is calculated by GEMS from the data at 25 °C according to:

$$\begin{aligned}\Delta_a G_T^o &= \Delta_f G_{T_0}^o - S_{T_0}^o (T-T_0) - \int_{T_0}^{T}\int_{T_0}^{T} \frac{C_p^o}{T}\,dT\,dT \\ &= \Delta_f G_{T_0}^o - S_{T_0}^o (T-T_0) - a_0\left(T\ln\frac{T}{T_0} - T + T_0\right) \\ &\quad -0.5a_1(T-T_0)^2 - a_2\frac{(T-T_0)^2}{2T\cdot T_0^2} - a_3\frac{2\left(\sqrt{T}-\sqrt{T_0}\right)^2}{\sqrt{T_0}}\end{aligned} \quad (1)$$

[29] where a_0, a_1, a_2, and a_3 are the empirical coefficients of the heat capacity equation $C_p^\circ = a_0 + a_1 T + a_2 T^{-2} + a_3 T^{-0.5}$, T_0 the reference temperature (298.15 K) and $S°$ the entropy. The apparent Gibbs free energy of formation $\Delta_a G_T^\circ$ refers to the free energies of the elements at 298 K. A more detailed description of the temperature corrections used in GEMS is given in Kulik [30] and in the online documentation of GEMS [26].

3.3. Thaumasite solubility as a function of temperature

Thaumasite $(CaSiO_3)_2(CaSO_4)_2\cdot(CaCO_3)_2\cdot 30H_2O$ has a structure similar to ettringite and is reported to form limited

Table 2
Standard thermodynamic properties of solids at 25 °C. All data with exception of thaumasite are taken from Lothenbach et al. [24]

	Log K_{S0} [a]	$\Delta_f G°$ [kJ/mol]	$\Delta_f H°$ [kJ/mol]	$S°$ [J/K/mol]	a_0 [J/K/mol]	a_1 [J/K^2/mol]	a_2 [JK/mol]	a_3 [J/K$^{0.5}$/mol]	$V°$ [b] [cm^3/mol]
Ettringite	−44.90	−15205.94	−17535	1900	1939	0.789			707
Thaumasite [c]	−49.40	−15128.46	−17373	1883	1860	0.703	−3.94e6	1600	663
C_3AH_6	−20.84	−5010.09	−5540	419	292	0.561			150
C_4AH_{13}	−25.40	−7326.55	−8302	700	711	1.047		−1600	274
C_2AH_8	−13.56	−4812.75	−5432	440	392	0.714		−800	184
$C_4A\overline{S}H_{12}$	−29.26	−7778.50	−8750	821	594	1.168			309
$C_4A\overline{C}H_{11}$	−31.47	−7337.46	−8250	657	618	0.982	−2.59e6		262
$C_4A\overline{C}_{0.5}H_{12}$	29.13	−7335.97	−8270	713	664	1.168	−1.30e6	−800	285
C_2ASH_8	−19.70	−5705.15	−6360	546	438	0.749	−1.13e6	−800	216
M_4AH_{10}	−56.02	−6394.56	−7196	549	−364	4.21	3.75e6	629 [d]	220
Brucite	−11.16	−832.23	−923	63	101	0.017	−2.56e6		25
$C_{1.67}SH_{2.1}$(jen.)	−13.17	−2480.81	−2723	140	210	0.120	−3.07e6		78
$C_{0.83}SH_{1.3}$(tob.)	−8.00	−1744.36	−1916	80	85	0.160			59
Portlandite	−5.20	−897.01	−985	83	187	−0.022	0	−1600	33
$SiO_{2,\ am}$	1.476	−848.90	−903	41	47	0.034	−1.13e6		29
Gypsum	−4.58	−1797.76	−2023	194	91	0.318			75
Anhydrite	−4.36	−1322.12	−1435	107	70	0.099			46
Calcite	−8.48	−1129.18	−1207	93	105	0.022	−2.59e6		37
$Fe(OH)_3$	−4.60	−711.61	−844	88	28	0.052			34
Al_2O_3	1.64	−1586.26	−1662	51	115	0.012	−3.51e6		26

a_0, a_1, a_2, a_3 are the empirical coefficients of the heat capacity equation: $C_p^\circ = a_0 + a_1 T + a_2 T^{-2} + a_3 T^{-0.5}$.

[a] All solubility products refer to the solubility with respect to the species $Al(OH)_4^-$, $Fe(OH)_4^-$, $SiO(OH)_3^-$, OH^-, H_2O, Ca^{2+}, Mg^{2+}, CO_3^{2-} or SO_4^{2-}.

[b] Molar volumes $V°$ at standard conditions were calculated from densities derived from crystallographic data.

[c] This paper; $V°$ calculated from unit cell given in Jacobson et al. [46].

[d] $C_p^\circ = a_0 + a_1 T + a_2 T^{-2} + a_3 T^{-0.5} - 0.00424 * T^2 + 2.11E{-}6 * T^3$.

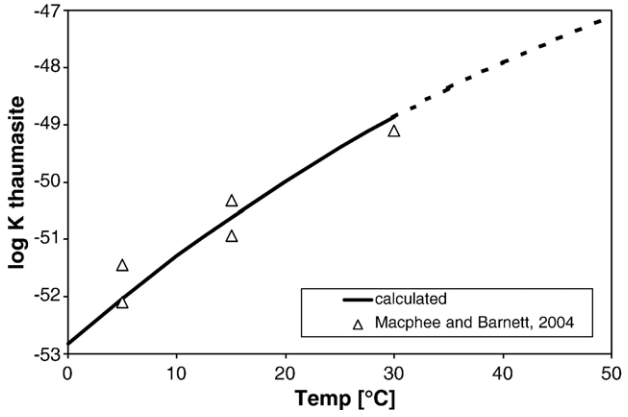

Fig. 2. Calculated solubility product of thaumasite as a function of temperature compared to solubility products derived from experimental data [31] according to the reaction $(CaSiO_3)_2(CaSO_4)_2(CaCO_3)_2 \cdot 30H_2O(s) \Leftrightarrow 6Ca^{2+} + 2H_3SiO_4^- + 2SO_4^{2-} + 2CO_3^{2-} + 2OH^- + 26H_2O$.

solid solution with ettringite. The solubility of synthetic thaumasite intermixed with ettringite has been measured by Macphee and Barnett [31]. For thaumasite from a geological source, a significantly lower solubility has been determined by Bellmann [32]. Based on the measured concentrations [31] in the presence of a thaumasite–ettringite mixture, a tentative solubility product of $10^{-49.4\pm1}$ was calculated for the reaction $(CaSiO_3)_2(CaSO_4)_2(CaCO_3)_2 \cdot 30H_2O(s) \Leftrightarrow 6Ca^{2+} + 2H_3SiO_4^- + 2SO_4^{2-} + 2CO_3^{2-} + 2OH^- + 26H_2O$ at 25 °C. As only a few solubility measurements in a relatively narrow temperature range are available (Fig. 2), the measured solubility data were not used for extrapolating these data to other temperatures but estimated entropy $S°$ and heat capacity $C_p°$ data were used. Entropy and heat capacity can be estimated using reference reactions based on structurally similar solids with known $S°$ and $C_p°$. If such reference reactions involve only solids and no "free" water, the change in heat capacity and the entropy equals approximately to zero [29,30,33]. Thus, $S°$ and $C_p°$ of thaumasite were estimated from the reference reaction $3CaO{\cdot}Al_2O_3 \cdot 3CaSO_4 \cdot 32H_2O(ettringite) + 2CaCO_3(calcite) + 2SiO_2(am) - 0.5CaSO_4 \cdot 2H_2O(gypsum) - 0.5CaSO_4(anhydrite) - Al_2O_3(s) - Ca(OH)_2(portlandite) \Leftrightarrow (CaSiO_3)_2(CaSO_4)_2(CaCO_3)_2 \cdot 30H_2O(thaumasite)$ resulting in $S° = 1883$ and $C_p° = 2118$ J/K/mol at 25 °C (see Table 2).

The solubility products calculated for thaumasite based on these estimated data agree well with the measured solubility products (Fig. 2). The saturation indices with respect to thaumasite are expressed as $\log(IAP/K_{S0})$, where the ion activity product IAP is calculated from the activities derived from the concentrations determined in the solution and K_{S0} is the solubility product of thaumasite. A positive saturation index implies oversaturation, a negative value undersaturation with regard to thaumasite.

4. Results and discussion

4.1. Initial hydrate phases

The hydrate phase assemblage of the laboratory cements before interaction with Na_2SO_4 solutions was calculated with GEMS [26] (see Subsystem E in Fig. 3a and b) assuming complete hydration of the cements. As input to the calculations the composition of the initial cements (HS, OPC) including the limestone was taken from Table 1. In the calculation the amount of sulfate present was varied from 0 to 20 wt.% SO_4^{2-} by weight cement paste. The initial hydrate phase assemblage in HS and OPC cement systems without limestone addition was calculated to be C–S–H, portlandite, ettringite, monosulfate, as well as traces of hemicarbonate and hydrotalcite (Figs. 3a, 4a). Both, the HS and the OPC cement clinkers contained small amounts of CO_2 resulting from production (Table 1).

With additional limestone in the HS and OPC cement system the hydrate phase assemblage was calculated to be C–S–H, portlandite, monocarbonate and traces of hydrotalcite and calcite (Figs. 3b, 4b). The modelled predictions agreed well with the experimental observations. In the HS and OPC cement systems without limestone addition (H0, P0) the presence of C–S–H, portlandite, ettringite, monosulfate and traces of hemicarbonate and hydrotalcite were observed by XRD

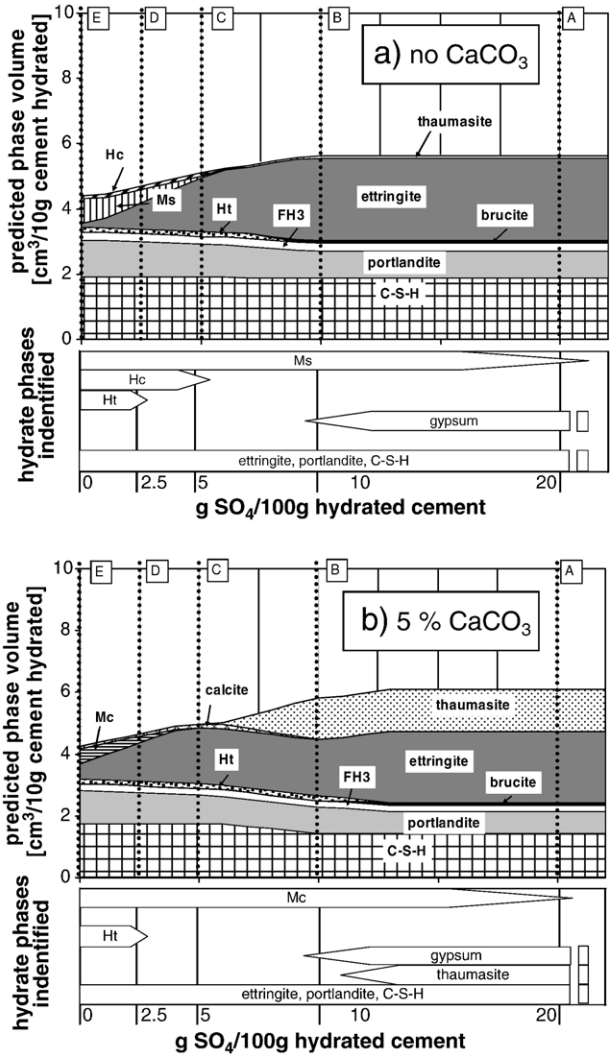

Fig. 3. Predicted and analysed solid phase assemblages for HS cement system with up to 5 wt.% limestone addition after 9 months sulfate interaction at 8 °C. Hc = hemicarbonate; Ht = hydrotalcite; Mc = monocarbonate; Ms = monosulfate; FH_3 = iron hydroxide.

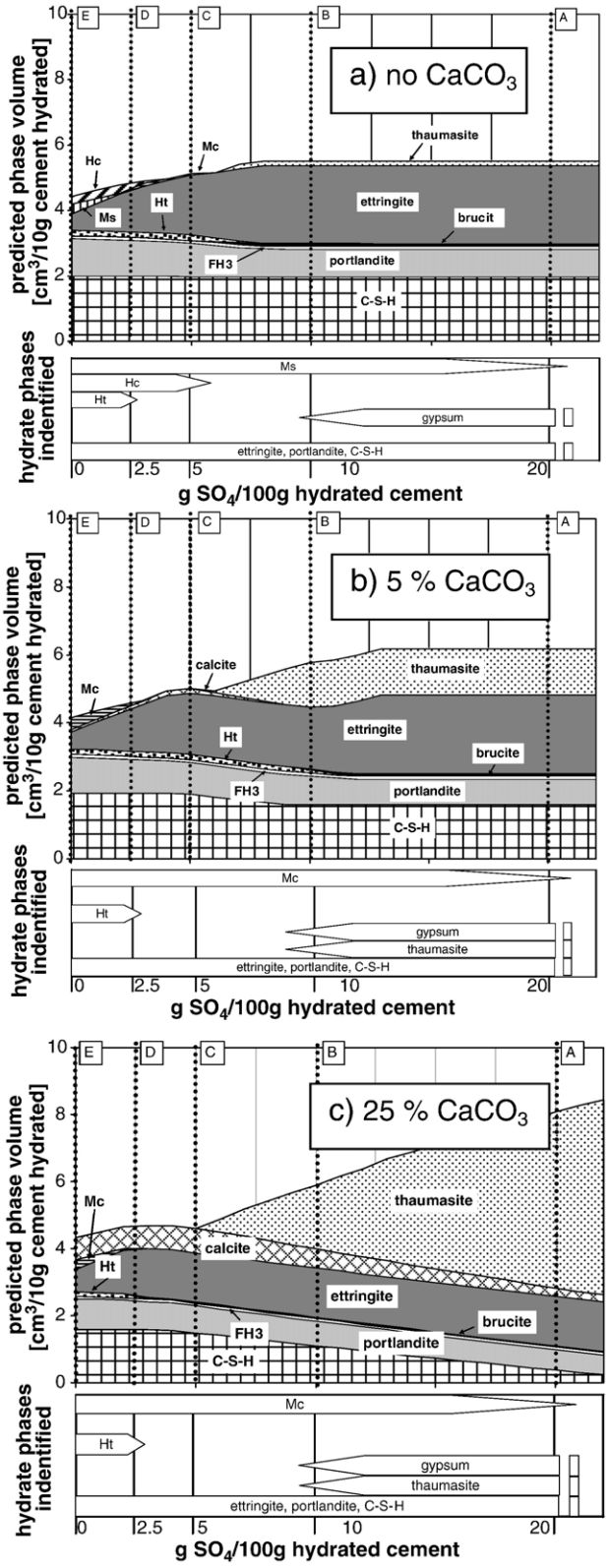

Fig. 4. Predicted and analysed solid phase assemblages for OPC cement systems with up to 25 wt.% limestone addition after 9 months sulfate interaction at 8 °C. Hc = hemicarbonate; Ht = hydrotalcite; Mc = monocarbonate; Ms = monosulfate; FH_3 = iron hydroxide.

(bottom part Figs. 3a, 4a). In the samples where limestone has been added (H5, P5, P25) the presence of monocarbonate and higher amounts of ettringite could be observed (bottom part Figs. 3b, 4b, c). Thus, the formation of monocarbonate and the persistence of ettringite agree with the observations of e.g. Kuzel and Pöllmann [15] and Bonavetti et al. [34].

4.2. Effect of sulfate interaction

If sulfate is progressively added to the subsystems moving from subsystem E to A thermodynamic modelling indicates that ettringite is formed at the expense of the AFm-phases (monosulfate, monocarbonate, hemicarbonate) until the aluminium available has been consumed, see Fig. 3 for HS and Fig. 4 for OPC cement. As before, the input for the calculations was the chemical composition of the initial binder systems given in Table 1.

Portlandite is predicted to be mainly consumed by the formation of ettringite and thaumasite. Thaumasite forms at the expense of portlandite, calcite and C–S–H in the presence of water. In the presence of more than 5 wt.% SO_4^{2-} by weight of cement paste (H5, P5), ettringite is the main Al-containing phase in all systems investigated, independent of the original composition of the cement. However, the composition of the cement has a large impact on the amount of thaumasite predicted to form. The calculations indicate that only the limestone containing cement systems, for both HS and OPC cement clinkers (high and low C_3A) can form significant amounts of thaumasite. In the absence of limestone (H0, P0) only traces of thaumasite can precipitate, see Figs. 3a, 4a. In the presence of 5 wt.% limestone (H5, P5), only a limited amount of thaumasite can form and obviously much more thaumasite forms if more limestone (P25) is present. Further, thaumasite formation is calculated to be limited by the C–S–H phase in the binder system and the amount of thaumasite is detrimental to the C–S–H content (Figs. 3 and 4).

It is interesting to note that thermodynamic modelling indicates that thaumasite becomes stable only above 5 wt.% SO_4^{2-} by weight of cement paste. Thaumasite is, from a thermodynamic point of view, only stable in a cement system if the available Al has been consumed by ettringite formation or in other words if the molar SO_3/Al_2O_3 ratio exceeds 3. These findings agrees with the observations reported by Juel et al. [21].

Experimentally, after sulfate interaction of 9 months, thaumasite was observed only in HS and OPC cement systems containing 5 or 25 wt.% limestone and in the presence of 10 or 20 wt.% sulfate, see lower parts of Figs. 3 and 4, Table 3). This observation agrees with the results of thermodynamic modelling and also with the observations of Juel et al. [21]. Smaller amounts of sulfate did not lead to thaumasite formation.

Thaumasite was identified in samples where limestone has been added to the cement, in both HS and OPC cement systems with low C_3A (H5) and high C_3A (P5, P25) content as shown in Fig. 5a, Table 3). The results agree quite well with the findings from Macphee [8] and Kalinowski and Trägardh [12] stating that minor amounts of carbonate in cements (5 wt.%) are sufficient to form thaumasite. Thaumasite could not be identified in samples without limestone addition, see Table 3.

Table 3
Pore solution compositions and phase assemblages after 9 months reaction time

Sample[i]			Solution composition [mmol/l][ii]					pH	Saturation indices for thaumasite[iv]	Phase assemblage	
			S[iii]	C[iii]	Ca	K	Na			Identified	Modelled
8 °C	H0	A	79	0.3	4.91	15.35	435	13.1	4.1	G Ett (Ms)	Ett (Th)
		B	33	0.3	6.61	14.84	204	13.0	5.0	(G) Ett Ms	Ett (Th)
	H5	A	76	0.4	4.57	14.07	422	13.0	4.1	G↓ Ett Th (Mc) Cc	Ett Th
		B	30	0.2	6.61	13.56	200	12.9	5.0	(G) Ett Mc Cc	Ett Th Cc
	P0	A	78	0.1	4.66	11.77	435	13.1	2.8	G Ett (Ms)	Ett (Th)
		B	33	0.3	5.86	11.76	200	13.0	4.9	(G) Ett Ms	Ett (Th)
	P5	A	76	0.2	4.57	10.49	426	13.0	3.3	G↓ Ett Th (Mc) Cc	Ett Th
		B	27	0.2	5.24	10.23	183	13.0	4.4	(G) Ett Th Mc Cc	Ett Th Cc
	P25	A	53	0.2	3.49	6.91	335	13.0	3.1	G↓ Ett Th (Mc) Cc	Ett Th Cc
		B	23	0.2	4.49	7.16	152	12.9	4.3	(G) Ett Th Mc Cc	Ett Th Cc
20 °C	H0	A	79	0.5	4.91	14.84	435	13.0	4.3	G↓ Ett (Ms)	Ett (Th)
		B	34	0.3	5.86	15.61	209	12.9	4.2	(G) Ett Ms	Ett (Th)
	H5	A	79	0.4	4.91	13.56	435	13.0	4.3	G↓ Ett (Mc) Cc	Ett Th
		B	31	0.4	5.74	13.81	191	12.9	4.7	(G) Ett Mc Cc	Ett Th Cc
	P0	A	79	0.3	4.57	12.26	435	13.0	3.3	G↓ Ett (Ms)	Ett (Th)
		B	31	0.4	5.11	12.28	204	13.0	4.4	(G) Ett Ms	Ett (Th)
	P5	A	78	0.3	4.32	10.47	426	13.0	3.3	G↓ Ett Th (Mc) Cc	Ett Th
		B	28	0.2	5.11	10.49	335	13.0	3.0	(G) Ett Th Mc Cc	Ett Th Cc
	P25	A	56	0.2	3.91	6.91	344	13.0	3.0	G↓ Ett Th (Mc) Cc	Ett Th Cc
		B	25	0.2	4.49	7.16	152	13.0	4.1	(G) Ett Th Mc Cc	Ett Th Cc

Portlandite, C–S–H and parts of clinker are present in all samples, Cc = Calcite; C = inorganic carbon; Ett = ettringite; G = gypsum; Mc = monocarbonate; Ms = monosulfate, S = sulfate; Th = thaumasite. ↓ = decreasing between 3 and 9 months; () = traces; [i]A: 20 wt.% SO_4^{2-}; B: 10 wt.% SO_4 by mass cement paste; [ii]measured Si and Al concentration were below the detection limit of 0.1 mmol/l; [iii]C = inorganic carbon, S = sulfate; [iv]Saturation index (thaumasite): SI = log (measured ion activity product / solubility product), see text. A positive saturation index indicates oversaturation.

The amount of C_3A present in the cement system did not result in any significant differences in thaumasite content. The peak intensities from XRD results after 9 months were more or less similar for both the OPC (7% C_3A) and the HS cement (0.4% C_3A), see Fig. 5a. Thus, it was not confirmed that the C_3A content accelerates thaumasite formation as suggested by Nobst and Stark [11].

Experimentally it was observed that at higher sulfate contents beside thaumasite and ettringite gypsum was also identified as a sulfate containing phase (Table 3, Figs. 3, 4). Between 3 and 9 months of sulfate interaction the amount of gypsum present decreased (Fig. 5b, Table 3). Gypsum seems to form as an intermediate sulfate phase parallel to or instead of thaumasite at high sulfate concentrations from the portlandite available as confirmed by an increase in pH and later acts as a source of sulfate applied for thaumasite formation as mentioned by Bellmann [35,32] and Irassar et al. [36]. In the experiments thaumasite was observed to be the last sulfate phase forming during sulfate interaction. In subsystems with high sulfate concentrations, i.e. subsystems A, B, where the formation of intermediate gypsum was observed, thermodynamic calculations predict that all sulfate available should be present as ettringite and thaumasite. This discrepancy between thermodynamic calculations and experimental results indicates that equilibrium has not been reached in the experiments but that probably different layers have been established in the crushed cement pastes.

The differences in the amounts of thaumasite formed at 8 °C with 5 wt.% (P5) or 25 wt.% (P25) limestone addition are up to 40%, whereas the difference between 10 wt.% (B) or 20 wt.% (A) sulfate addition is almost negligible, see experimental data reported in Fig. 6. In comparison to the findings from Hartshorn et al. [20] and Kalinowski and Trägardh [12] increasing amounts of sulfate concentration (subsystems A, B) did not increase thaumasite formation, whereas higher amounts of limestone filler (P5, P25) increased the amount of thaumasite formed during the 9 months of sulfate interaction. This indicates that in the systems investigated here the limiting factor for thaumasite formation is the quantity of carbonate present. Smaller amounts of sulfate present in the subsystems, e.g. subsystems C, D with ≤ 5 wt.% SO_4 by weight cement paste did not lead to thaumasite formation (Figs. 3 and 4).

The experimental data show that some of the AFm-phases (monosulfate, monocarbonate) formed during hydration persist during sulfate interaction (Figs. 3, 4 and Table 3) in contrast to the model predictions. This indicates that even though the hydrated cement was ground to 0.5–2.0 mm, equilibrium has not been reached. Obviously, the reactions did not occur throughout the whole cement paste grains but layers have been established within the crushed cement paste. In fact, microstructural investigations [37], showed the formation of such layers in cement paste. In the outer 40 μm the presence of ettringite and gypsum could be observed, while portlandite was depleted. In the core of the cement paste grains (>0.25 mm), the composition was not altered even after 9 months. These findings showed that after 9 months the PEA method was between pure equilibrium batch test and diffusion-limited external sulfate attack on mortar bars. The formation of such layers is consistent with the observations of Irassar et al. [36] and Planel et al. [38] who observed in mortar samples the formation of distinct layers

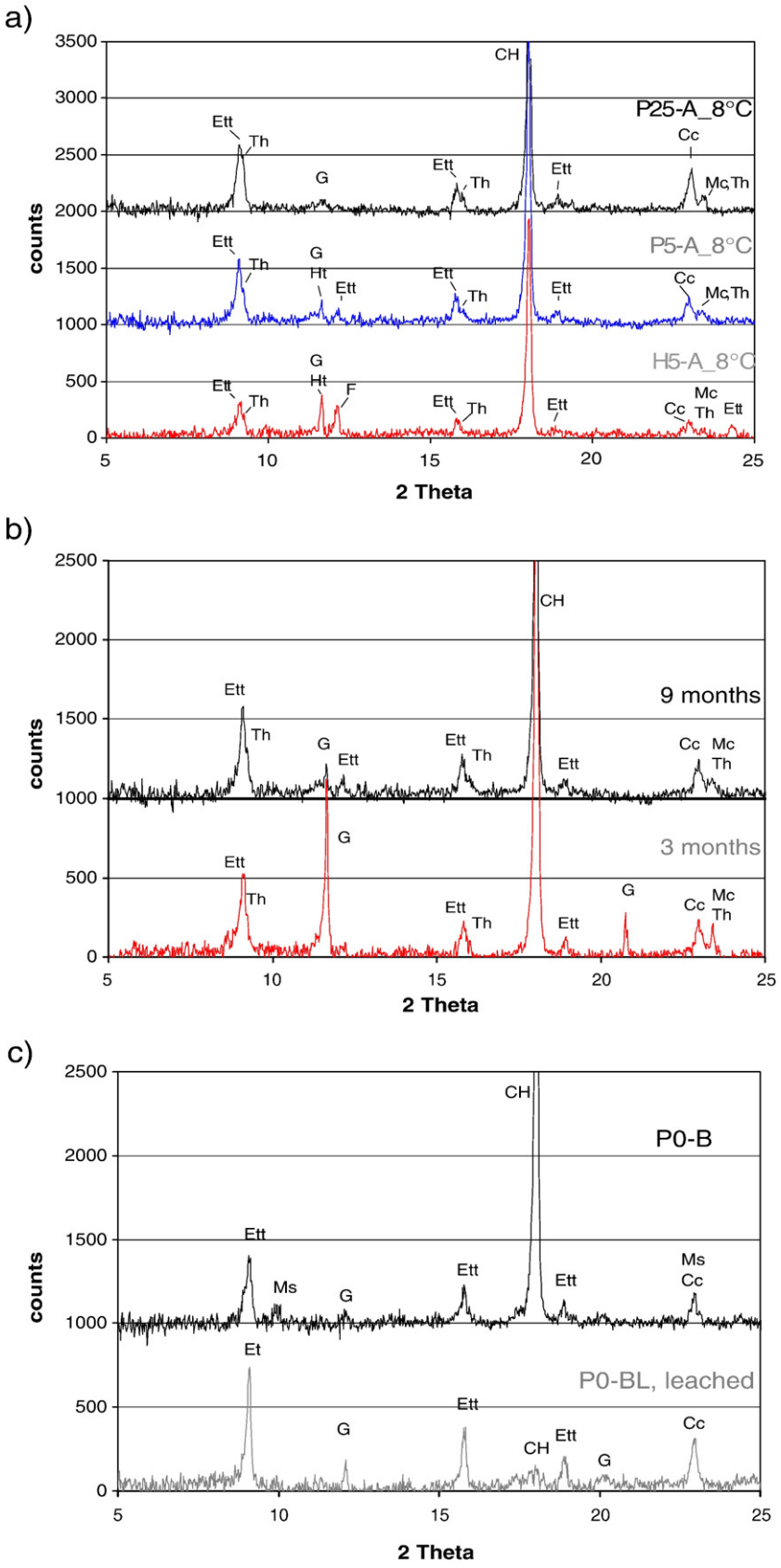

Fig. 5. a–c: XRD results of a) H5, P5 and P25 from subsystem A with 20 wt.% sulfate after 9 months; of b) P5 after 3 and 9 months sulfate interaction at 8 °C and c) P0 with or without leaching at 8 °C after 9 months. CH = portlandite, Cc = calcite, Ett = ettringite; F = Ferrite, G = gypsum; Ht = hydrotalcite; Mc = monocarbonate, Ms = monosulfate, Th = thaumasite.

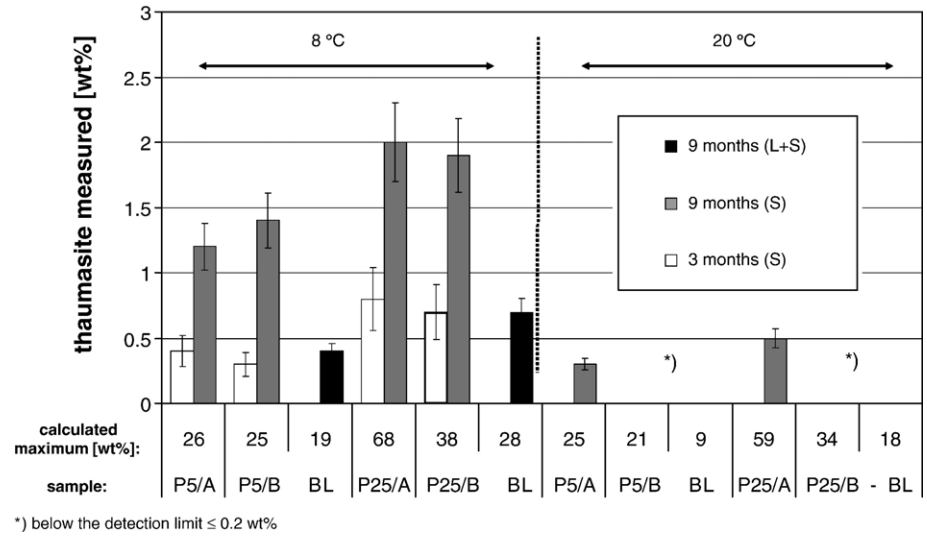

Fig. 6. Quantitative concentrations of thaumasite obtained from NMR spectroscopy in selected experiments of OPC cement systems after 3 and 9 months of sulfate interaction (*S*) and leaching and sulfate interaction (*L*+*S*) in relation to the predicted maximum amounts.

near the surface of samples exposed to sodium sulfate solutions. They described both the presence of a moving reaction front where ettringite and gypsum is formed.

4.3. Effect of temperature

To take into account the temperature aspect the phase assemblage was modelled at 8 °C and 20 °C for an OPC cement containing 25 wt.% limestone (Figs. 4c, 7). In both cases the formation of thaumasite was calculated at higher sulfate concentrations and in the presence of limestone. However, at 20 °C (Fig. 7) somewhat less thaumasite was calculated to form than at 8 °C (Fig. 4c). This is due to relatively strong increase of the solubility of thaumasite with increasing temperature as illustrated in Fig. 2 and to the high water/solid ratio used in the experiments. However, it would not be observed at low liquid/solid ratio since the solution would rapidly be supersaturated with respect to thaumasite, which would precipitate. The thermodynamic calculations are in good agreement with the findings from other investigations indicating that thaumasite is more stable at lower temperatures as suggested by Bensted et al. [2,3]. Based on the thermodynamic data it is calculated that thaumasite could persist under the conditions used in the experiments up to a temperature of approximately 45 °C. The calculations indicate that the temperature up to which thaumasite is thermodynamically stable depends strongly on the pH. Higher pH values as present in the pore solution of hydrated cements which have interacted with less Na_2SO_4 solution, leads to a strong decrease of dissolved calcium and thus destabilises thaumasite at lower temperatures. Cements interacting with higher amounts of sulfate containing solutions will exhibit a lower pH and in such systems thaumasite will be stable at even higher temperatures.

The quantities of thaumasite determined by Si–NMR for OPC cement systems (Fig. 6) show that thaumasite was detectable after 3 months of sulfate interaction at 8 °C. At 20 °C only very small amounts of thaumasite could be detected by Si–NMR even after 9 months of sulfate interaction. Furthermore, at 8 °C, significantly more thaumasite was experimentally detected although in the comparable OPC cement systems with 5 or 25 wt.% limestone additions, similar amounts of thaumasite have been calculated. The computation of the saturation indices for thaumasite from the measured concentrations showed slightly higher degrees of oversaturation with respect to thaumasite at 8 °C than at 20 °C (Tables 3 and 5). This difference, however, is rather small indicating that not only thermodynamics but also kinetics determines the amount of thaumasite formed and that the formation of thaumasite is faster at 8 °C than at 20 °C.

The observations of thaumasite formation at 20 °C in the laboratory cements investigated are in good agreement to the

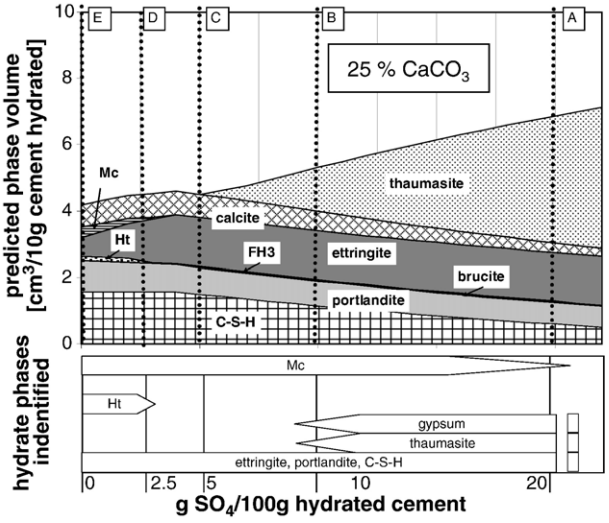

Fig. 7. Sulfate interaction comparing experimental and predicted solid phase assemblage for an OPC cement system with 25 wt.% limestone addition at 20 °C. Ht = hydrotalcite; Mc = monocarbonate; FH_3 = iron hydroxide.

observation of thaumasite formation at 20 °C and above in Italy and Southern California [6,7]. Generally, the amount of thaumasite determined by Si–NMR is only a small portion of what is predicted from the thermodynamic data, indicating that thaumasite formation is kinetically very slow. In fact thaumasite is the last sulfate phase forming during sulfate interaction due to its slow reaction kinetics which agrees to the observations of Köhler et al. [39] and Barnet et al. [40]. The thermodynamic calculations further show that thaumasite is the end product in the cement systems studied.

In the experiments, after 9 months, equilibrium has not been reached. Thermodynamic modelling, however, can be used to assess the total potential risk of the binder systems for thaumasite formation with respect to temperature and sulfate concentration.

4.4. Influence of leaching

The influence of leaching on the formation of thaumasite was calculated for leached and unleached OPC cement system with 25 wt.% limestone for the sulfate uptake at 8 °C (Figs. 4c, 8). The phase assemblage for the leached OPC cement was modelled using the composition of the laboratory cements after the leaching process as given in Table 1.

The calculation indicates that the leached OPC cement system before the addition of sulfate consists of C–S–H, ettringite, AFm (e.g. monocarbonate) and traces of hydrotalcite as stable phases, given for a calcium carbonate containing cement (Fig. 8). The main difference to the unleached OPC cement system is the absence of portlandite as well as the presence of C–S–H with a lower Ca/Si ratio.

With sulfate progressively added to the cement system the modelled data indicate that as already observed in the leached OPC samples relatively more ettringite is present (Fig. 8)

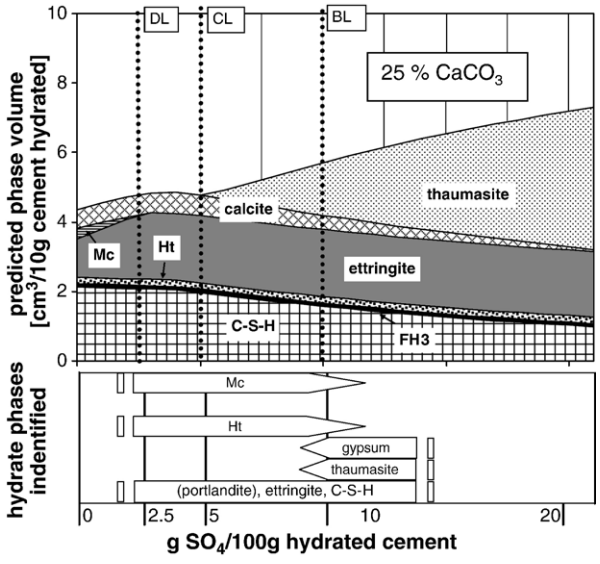

Fig. 8. Sulfate interaction comparing experimental and predicted solid phase assemblages for an OPC cement system with 25 wt.% limestone addition at 8 °C subsequent to leaching. Ht = hydrotalcite; Mc = monocarbonate; FH_3 = iron hydroxide.

Table 4
Total porosity and portlandite content of the laboratory cement pastes before and after leaching

Sample	$Ca(OH)_2$ content [a] [wt.%]					Total porosity [b]				
	H0	H5	P0	P5	P25	H0	H5	P0	P5	P25
Initial	15	14	15	14	12	18	17	15	14	20
Leached	2	2	3	3	1	36	35	28	27	39

[a] Obtained from thermogravimetric analysis TGA.
[b] Obtained from mercury intrusion MIP.

compared to the non leached experiments (Fig. 4c). The fraction of aluminium present in the leached systems is higher, as a part of the calcium is removed during leaching. The calculations further show that in the presence of sulfate, additional ettringite is formed at the expense of the AFm-phases consuming the available aluminium resources (Fig. 8). The modelled hydrate phase assemblage indicates that less thaumasite is formed in leached conditions.

The experimental results show that in leached HS and OPC cement systems before the addition of sulfate the chemical composition and the pore structure change. After leaching for 4 months the amount of calcium (≥50 wt.%) and alkalis (≥90 wt.%) are strongly reduced whereas the amounts of silicate, aluminium and iron remained nearly constant (Table 1). In addition, during the leaching a small uptake of CO_2 into the cement systems is observed.

Portlandite was reduced by more than 80 wt.% during the leaching process as shown in Table 4. However, small amounts of portlandite (1–3 wt.%) were still present indicating that the leaching process was not completed after 4 months. The MIP measurements of samples before and after leaching showed that the total porosity almost doubled (Table 4). The pore size distribution in the investigated samples shows significantly more small pores ≤10 nm and more pores between 10 – 100 nm to be present in the leached samples (Fig. 9). The increase in pore volume can be attributed to the dissolution of the large crystals of portlandite $Ca(OH)_2$ [41–44]. The dissolution of Ca from the C–S–H might explain the increase the amount of small pores, although this could also be due to the removal of portlandite facilitating access to the small pores [38,45].

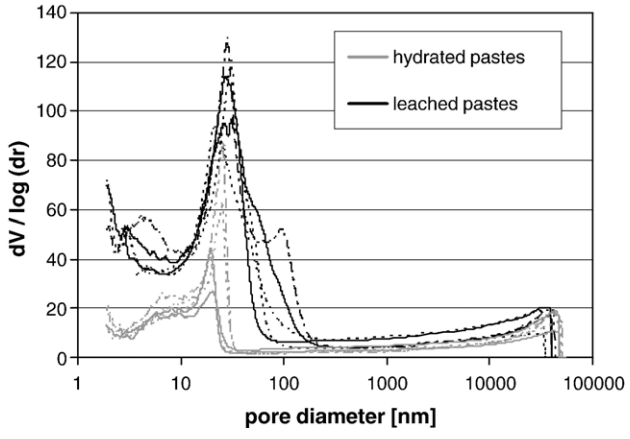

Fig. 9. MIP pore size distribution of hydrated and leached HS and OPC cement pastes.

The experimental results of the leached samples indicate that with 2.5 wt.% sulfate addition ettringite, monocarbonate and traces of hydrotalcite are present, see bottom part of Fig. 8, subsystem DL. With more sulfate added to the cement systems more ettringite is present than in the non leached experiments (Fig. 5c). These observations agree with the calculated data. In addition, the increase of porosity in the leached systems can enhance sulfate interaction and thus ettringite formation due to faster diffusion into the grains.

The Si–NMR results show that significantly less thaumasite was formed in the leached OPC cement systems with high C_3A content (P5, P25) as shown in Fig. 6. Thaumasite could not be identified in the leached HS cement systems with low C_3A content (H0, H5) after 9 months of sulfate interaction which is in contrast to the non leached systems (Table 5) where thaumasite was observed. These findings agree with the observations of Zhou and Sharp [17], who found decreasing amounts of thaumasite with decreasing pH but it is in contrast to the conclusions of Romer et al. [13], who suggested that leaching facilitates thaumasite formation.

Although, leaching increased the porosity of the OPC cement pastes and therefore accelerates sulfate interaction, thaumasite formation is not enhanced. Thaumasite formation was found to be even slower in leached samples than in non leached samples at the same sulfate concentrations and exposition time. This indicates that the precipitation kinetics of thaumasite might not only be diffusion controlled but also influenced by the different mineralogical composition of the cement systems under these conditions.

The XRD results show that slightly more gypsum is present in leached subsystems with 10 wt.% sulfate addition compared to the unleached subsystems (Fig. 5c) due to the very slow thaumasite formation. As most of the portlandite has been removed from these systems, this formation of gypsum implies decalcification of the C–S–H. Although slower than in the unleached samples, thaumasite formation in the leached OPC cement systems is still faster at 8 °C than 20 °C (Fig. 6).

4.5. Composition of reaction solutions

Beside the solid phases the composition of the reaction solutions of the PEA experiments was also investigated. The composition of the solution was calculated by thermodynamic modelling for all experiments at 8 and 20 °C. The calculated concentrations of selected ions for an OPC cement system with 25 wt.% limestone addition are given in Fig. 10.

In the subsystems where no sulfate was added, the calculated solution compositions are dominated by OH^-, Ca, K and Na. The addition of Na_2SO_4 leads not only to an increase in the calculated sodium and sulfate concentrations but also to an increase of the hydroxide concentration as a part of the sulfate added precipitates as sulfate containing phases. The concentration of Ca which is determined by the presence of $Ca(OH)_2$, decreases accordingly (Fig. 10a).

The concentrations of ions in solution were measured after 3 and 9 months. In Fig. 10a the data for an OPC with 25 wt.% limestone addition are compared to the modelled concentrations assuming equilibrium. The concentrations measured in the subsystems without sulfate addition agree well with the modelled data. The addition of sulfate leads to a significant difference between calculated and measured data. The observed trends of the measured ion concentrations over time indicate an evolution towards the predicted ion concentrations. After 9 months, only a fraction of sulfate added to the subsystems has been consumed due to the formation of ettringite and thaumasite; gypsum has precipitated instead. At higher sulfate additions, the measured Ca^{2+} and SO_4^{2-} concentrations are buffered by the gypsum present. This indicates that equilibrium has not yet been reached after 9 months of sulfate interaction.

The composition of the reaction solutions for the leached cement systems containing 25 wt.% limestone is reproduced in Fig. 10b. The prediction indicates that leaching reduces the concentration of Ca, Na and K as well as OH^- in the solution. The carbonate, aluminium and silicate concentrations in the solution are calculated to be higher in leached than in non leached systems (Fig. 10a, b).

Table 5
Pore solution compositions and phase assemblages for sulfate interaction (9 months) subsequent to leaching

Sample[i]			Solution composition [mmol/l][ii]					pH	Saturation indices for thaumasite[iv]	Phase assemblage	
			S[iii]	C[iii]	Ca	K	Na			Identified	Modelled
8 °C	H0	BL	33	0.8	0.87	0.16	169	12.5	4.1	G Ett Ms (Cc)	Ett (Th)
	H5	BL	33	1.2	0.50	0.21	157	12.4	3.3	G Ett Mc Cc↑	Ett Th Cc
	P0	BL	33	1.0	0.55	0.25	169	12.7	3.2	G Ett Ms (Cc)	Ett (Th)
	P5	BL	29	1.0	0.52	0.28	157	12.7	3.1	G Ett Th Mc Cc↑	Ett Th Cc
	P25	BL	29	1.4	0.40	0.10	122	12.5	3.1	G Ett Th Mc Cc↑	Ett Th Cc
20 °C	H0	BL	31	0.8	0.72	0.20	169	12.6	3.0	G Ett Ms (Cc)	Ett (Th)
	H5	BL	33	1.0	0.42	0.25	161	12.7	2.0	G Ett Ms Cc↑	Ett Th Cc
	P0	BL	33	0.8	0.62	0.33	174	12.7	2.5	G Ett Ms (Cc)	Ett (Th)
	P5	BL	29	0.8	0.62	0.38	165	12.8	2.6	G Ett (Th) Cc↑	Ett Th Cc
	P25	BL	27	1.0	0.50	0.12	122	12.6	2.8	G Ett (Th) Mc Cc↑	Ett Th Cc

Portlandite and C–S–H present in all samples, Cc = Calcite; Ett = ettringite; G = gypsum; Mc = monocarbonate; Ms = monosulfate, S = sulfate; Th = thaumasite. ↑ = increasing after leaching; () = traces; [i]BL: 10 wt.% SO_4 by mass cement paste; [ii]measured Si and Al concentration were below the detection limit of 0.1 mmol/l; [iii]C = inorganic carbon, S = sulfate; [iv]Saturation index (thaumasite): SI=log (measured ion activity product/solubility product), see text. A positive saturation index indicates oversaturation.

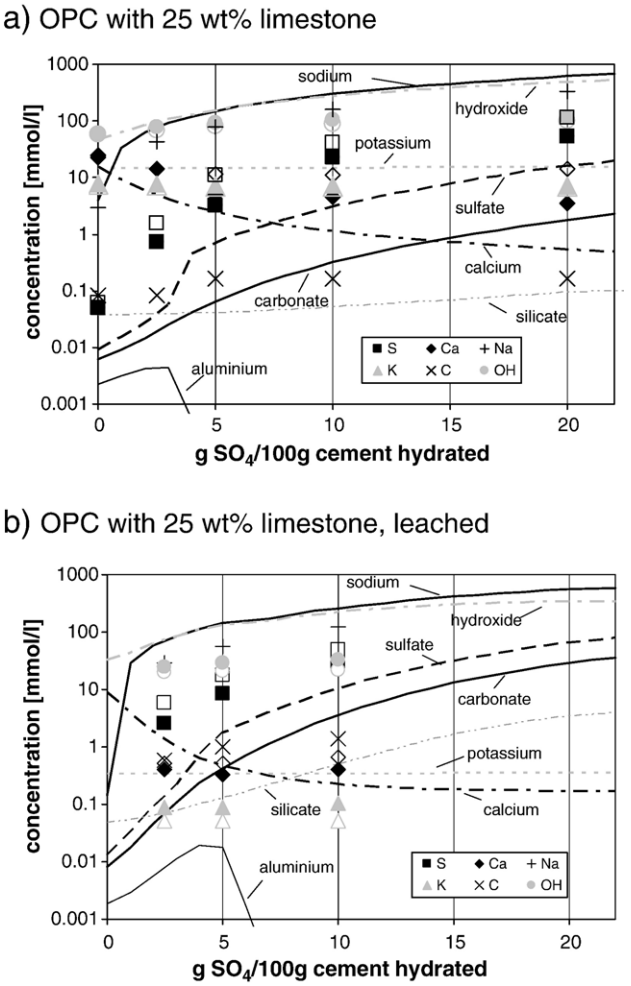

Fig. 10. Predicted and experimental composition of the pore solution of an OPC cement system with 25 wt.% limestone addition analysed after 3 months (empty symbols) and 9 months (filled symbols) sulfate interaction.

The concentrations of Ca, Na and K as well as OH^- where found to be significantly lower in the experiments undergoing leaching before sulfate interaction (Fig. 10b). This is due to the fact that portlandite and alkalis are reduced in the leached cement systems as mentioned in 4.4 and agrees with modelling data. The concentration of carbonate in solution was determined to be slightly increased as indicated by the modelled data. Also for the leached systems the experimental data for the pore solution composition reproduces the trends which were predicted by the thermodynamic model.

Generally, in the absence of sulfate and at low sulfate concentration modelled and measured data agreed well. In the subsystems where sulfate was added, modelled and measured data did not yet agree after 9 months indicating that equilibrium has not been reached.

5. Conclusions

Limestone addition influences the hydrate phase assemblage in hydrated cements. In the presence of limestone, monocarbonate and ettringite are present instead of monosulfate. In cement systems with very little carbonate, hemicarbonate may form.

Under sulfate exposure AFm-phases (monosulfate, hemicarbonate in the absence of carbonate and monocarbonate in the presence of carbonate) react to form ettringite. Thaumasite precipitates at high levels of added sulfate. Experimental data as well as thermodynamic modelling indicate, that thaumasite can only be formed under conditions where the molar SO_3/Al_2O_3 ratio in the cement system exceeds 3. For lower amounts of SO_3 only ettringite is formed.

In Portland cement systems with 5 wt.% limestone addition, the amount of calcite limits the extent of thaumasite formation if more than approximately 10 wt.% SO_4^{2-} is present. In the case of 25 wt.% limestone addition much more thaumasite can be formed. Beside the influence of the carbonate, thaumasite formation is also limited by the C–S–H phase of the Portland cement systems.

Gypsum was observed to form parallel to or instead of thaumasite at high sulfate concentrations. In the experiments gypsum was formed initially since the formation of thaumasite is kinetically very slow. Gypsum acts later as a source of sulfate for the precipitation of additional thaumasite. Thaumasite was found to be the last sulfate phase to form during sulfate interaction due to kinetic reasons.

The experimental results further show that thaumasite formation may occur in limestone containing cement systems with both high and low C_3A content. The C_3A content was not found to have a significant influence on thaumasite formation.

Thermodynamically, slightly higher amounts of thaumasite were calculated to be stable at lower temperatures. In addition, the experiments show that kinetic effects are dominant; at lower temperature thaumasite is formed much faster.

Leaching reduced the amount of portlandite and increased the porosity of the cement paste systems. Furthermore leaching reduced the amount of alkalis and calcium in the cement systems resulting in lower pH values in the reaction solution. Thaumasite was also formed in leached cement systems. However, experimental and modelling results show that in leached cement systems the amount of thaumasite formed is smaller than in unleached cement systems, whereas secondary gypsum and ettringite formation are favoured under these conditions.

The progressive equilibrium approach PEA used to investigate the chemical aspects of sulfate attack is a good tool for simulating various levels of sulfate uptake due to an external sulfate attack. Generally, thaumasite was detected were it was modelled to be stable in significant amounts. However, the experimental setup, especially the selection of a *w/c* ratio of 0.35 in this study did not allow equilibrium conditions to be reached after 9 months of sulfate interaction at a liquid/solid ratio of 7. If the experiments are applied properly equilibrium in the samples can be reached within months to years. The approach to equilibrium would be faster if a higher *w/c* ratio and if an even finer fraction of paste particles would be used. Thus, the small paste particle size should minimize the diffusion compared to diffusion controlled experiments.

Acknowledgements

The authors would like to thank L. Brunetti, W. Trindler, O. Nagel, U. Gfeller, E. Gallucci and J. Kaufmann for their assistance

in the experimental part of this study. Special thanks to Cemsuisse, the association of the Swiss Cement Industry for financial support.

References

[1] The Thaumasite Expert Group, The thaumasite form of sulfate attack: risks, diagnosis, remedial works and guidance on new constructions, Department of the Environment, Transport London, 1999.

[2] J. Bensted, Mechanism of thaumasite sulphate attack in cements, mortars and concretes, Zem.-Kalk-Gips 53 (2000) 704–709.

[3] J. Bensted, Thaumasite — background and nature in deterioration of cements, mortars and concretes, Cem. Concr. Compos. 21 (2) (1999) 117–121.

[4] N.J. Crammond, The thaumasite form of sulfate attack in the UK, Cem. Concr. Compos. 25 (8) (2003) 809–818.

[5] N.J. Crammond, M.A. Halliwell, The thaumasite form of sulfate attack in concretes containing a source of carbonate ions — a microstructural overview, International Symposium for Advances in Concrete Technology, 1995.

[6] S. Diamond, Thaumasite in Orange County, Southern California: an inquiry into the effect of low temperature, Cem. Concr. Compos. 25 (8) (2003) 1161–1164.

[7] M. Collepardi, Thaumasite formation and deterioration in historic buildings, Cem. Concr. Compos. 21 (2) (1999) 147–154.

[8] D. Macphee, S. Diamond, Thaumasite in cementitious materials, Cem. Concr. Compos. 25 (8) (2003) 805–807.

[9] M.T. Blanco-Varela, J. Aguilera, S. Martinez-Ramirez, Effect of cement C3A content, temperature and storage medium on thaumasite formation in carbonated mortars, Cem. Concr. Compos. 36 (4) (2006) 707–715.

[10] P. Brown, R.D. Hooton, Ettringite and thaumasite formation in laboratory concretes prepared using sulfate-resisting cements, Cem. Concr. Compos. 24 (3–4) (2002) 361–370.

[11] P. Nobst, J. Stark, Investigations on the influence of cement type on thaumasite formation, Cem. Concr. Compos. 25 (8) (2003) 899–906.

[12] M. Kalinowski, J. Trägardh, Thaumasite and gypsum formation in SCC with sulfate resistant cement exposed to a moderate sulfate concentration, Second North American Conference on the Design and Use of Self-Consolidating Concrete, 2005, pp. 319–325, (3).

[13] M. Romer, L. Holzer, M. Pfiffner, Swiss tunnel structures: concrete damage by formation of thaumasite, Cem. Concr. Compos. 25 (8) (2003) 1111–1117.

[14] G. Collett, N.J. Crammond, R.N. Swamy, J.H. Sharp, The role of carbon dioxide in the formation of thaumasite, Cem. Concr. Res. 34 (2004) 1599–1612.

[15] H.-J. Kuzel, H. Pöllmann, Hydration of C3A in the presence of Ca(OH)2, CaSO4 · 2H2O and CaCO3, Cem. Concr. Res. 21 (5) (1991) 885–895.

[16] D.W. Hobbs, M.G. Taylor, Nature of the thaumasite sulfate attack mechanism in field concrete, Cem. Concr. Res. 30 (4) (2000) 529–533.

[17] Q. Zhou, J. Hill, E.A. Byars, J.C. Cripps, C.J. Lynsdale, J.H. Sharp, The role of pH in thaumasite sulfate attack, Cem. Concr. Res. 36 (1) (2006) 160–170.

[18] M.E. Gaze, N.J. Crammond, The formation of thaumasite in a cement: lime:sand mortar exposed to cold magnesium and potassium sulfate solutions, Cem. Concr. Compos. 22 (3) (2000) 209–222.

[19] M.E. Gaze, The effects of varying gypsum content on thaumasite formation in a cement:lime:sand mortar at 5 °C, Cem. Concr. Res. 27 (2) (1997) 259–265.

[20] S.A. Hartshorn, J.H. Sharp, R.N. Swamy, The thaumasite form of sulfate attack in Portland-limestone cement mortars stored in magnesium sulfate solution, Cem. Concr. Compos. 24 (3–4) (2002) 351–359.

[21] I. Juel, D. Herfort, R. Gollop, J. Konnerup-Madsen, H.J. Jakobsen, J. Skibsted, A thermodynamic model for predicting the stability of thaumasite, Cem. Concr. Compos. 25 (8) (2003) 867–872.

[22] J. Skibsted, S. Rasmussen, D. Herfort, H.J. Jakobsen, 29Si cross-polarization magic-angle spinning NMR spectroscopy—an efficient tool for quantification of thaumasite in cement-based materials, Cem. Concr. Compos. 25 (8) (2003) 823–829.

[23] J. Skipsted, L. Hjorth, H.J. Jakobsen, Quantification of thaumasite in cementitious materials by 29Si{1H} cross-polarisation magic-angle spinning NMR spectroscopy, Adv. Cem. Res. (7) (1995) 69–83.

[24] B. Lothenbach, T. Matschei, G. Möschner, F.P. Glasser, Thermodynamic modelling of the effect of temperature on the hydration and porosity of Portland cement, Cem. Concr. Res. 38 (1) (2008) 1–18.

[25] B. Lothenbach, F. Winnefeld, Thermodynamic modelling of the hydration of Portland cement, Cem. Concr. Res. 36 (2) (2006) 209–226.

[26] D. Kulik, GEMS-PSI 2.1, PSI, Villigen, Switzerland, 2006 available at http://leswebpsi.ch/software/GEMS-PSI.

[27] W. Hummel, U. Berner, E. Curti, F.J. Pearson, T. Thoenen, Nagra/PSI Chemical Thermodynamic Data Base 01/01, University Publishers/ uPUBLISH.com, USA, also published as Nagra Technical Report NTB 02–16, Wettingen, Switzerland. 2002.

[28] T. Thoenen, D. Kulik, Nagra/PSI chemical thermodynamic database 01/01 for the GEM-Selektor (V.2-PSI) geochemical modeling code, PSI, Villigen, 2003 available at http://les.web.psi.ch/software/GEMS-PSI/doc/pdf/TM-44-03-04-web.pdf.

[29] G.M. Anderson, D.A. Crerar, Thermodynamics in geochemistry: the equilibrium model, Oxford University Press, Oxford, 1993.

[30] D. Kulik, Minimising uncertainty induced by temperature extrapolations of thermodynamic data: a pragmatic view on the integration of thermodynamic databases into geochemical computer codes, The Use of Thermodynamic Databases in Performance Assessment, OECD, Barcelona, 2002, pp. 125–137.

[31] D.E. Macphee, S.J. Barnett, Solution properties of solids in the ettringite–thaumasite solid solution series, Cem. Concr. Res. 34 (2004) 1591–1598.

[32] F. Bellmann, On the formation of thaumasite part I, Adv. Cem. Res. 16 (2) (2004) 55–60.

[33] Y.D. Gu, M.S. Gammons, M.S. Bloom, A one-term extrapolation method for estimating equilibrium constants of aqueous reactions at elevated temperatures, Geochim. Cosmochim. Acta 58 (17) (1994) 3545–3560.

[34] V.L. Bonavetti, V.F. Rahhal, E.F. Irassar, Sudies on the carboaluminate formation in limestone filler-blended cements, Cem. Concr. Res. 31 (2001) 853–859.

[35] F. Bellmann, On the formation of thaumasite CaSiO3CaSO4CaCO315H2O Part II, Adv. Cem. Res. 16 (2004) 89–94.

[36] E.F. Irassar, M.A. Bonavetti, M.A. Trezza, M. Gonzalez, Thaumasite formation in limestone filler cements exposed to sodium sulphate solution at 20 °C, Cem. Concr. Compos. 27 (2005) 77–84.

[37] T. Schmidt, Sulfate attack and the role of internal carbonate on the formation of thaumasite. PhD thesis, École Polytechnique Fédérale de Lausanne, Lausanne, 2007.

[38] D. Planel, J. Sercombe, P. Le Besop, F. Adenot, J.M. Torrenti, Long-term performance of cement paste during combined calcium leaching-sulfate attack: kinetics and size effect, Cem. Concr. Res. 36 (2006) 137–143.

[39] S. Köhler, D. Heinz, L. Urbonas, Mechanismus der Thaumasitbildung in verschiedenen Bindemittelsystemem, Ibausil, 2003, pp. 0711–0718, (2).

[40] S.J. Barnett, C.D. Adam, A.R.W. Jackson, Solid solutions between ettringite and thaumasite, Mater. Sci. 35 (2000) 4109–4114.

[41] A. Muberra, F.P. Glasser, Long-term leaching mechanisms of Portland cement-stabilized municipal solid waste fly ash in carbonated water, Cem. Concr. Res. 29 (2) (1999) 179–186.

[42] S. Catinaud, J.J. Beaudoin, J. Marchand, Influence of limestone addition on calcium leaching mechanisms in cement-based materials, Cem. Concr. Res. 30 (12) (2000) 1961–1968.

[43] K. Haga, M. Shibata, M. Hironaga, S. Tanaka, S. Nagasaki, Change in pore structure and composition of hardened cement paste during the process of dissolution, Cem. Concr. Res. 35 (5) (2005) 943–950.

[44] K. Haga, S. Sutou, M. Hironaga, S. Tanaka, S. Nagasaki, Effects of porosity on leaching of Ca from hardened ordinary Portland cement paste, Cem. Concr. Res. 35 (9) (2005) 1764–1775.

[45] C. Galle, H. Peycelon, P. Le Bescop, Effect of an accelerated chemical degradation on water permeability and pore structure of cement-based materials, Adv. Cem. Res. 16 (2004) 105–114.

[46] S.D. Jacobsen, J.R. Smyth, R.J. Swope, Thermal expansion of hydrated six-coordinate silicon in thaumasite, Ca3Si(OH)6(CO3)(SO4)12H2O, Phys. Chem. Min. 30 (6) (2003) 321–329.